Geophysical Research Letters

RESEARCH LETTER
10.1029/2024GL110839

Plasma Sheet Magnetic Flux Transport During Geomagnetic Storms

Savvas Raptis[1], **Viacheslav Merkin**[1], **Shinichi Ohtani**[1], **Matina Gkioulidou**[1], and **Leonardo H. Regoli**[1]

[1]Johns Hopkins University Applied Physics Laboratory, Laurel, MD, USA

Key Points:

- Convection electric field is elevated across the plasma sheet during storms, but convection properties are different between dawn and dusk
- Dawn magnetic flux transport during storm time is statistically associated with relatively faster flows
- Dusk magnetic flux transport during storm times is statistically associated with more dipolar magnetic fields

Supporting Information:

Supporting Information may be found in the online version of this article.

Correspondence to:

S. Raptis,
savvas.raptis@jhuapl.edu;
savvasraptis@pm.me

Citation:

Raptis, S., Merkin, V., Ohtani, S., Gkioulidou, M., & Regoli, L. H. (2024). Plasma sheet magnetic flux transport during geomagnetic storms. *Geophysical Research Letters*, *51*, e2024GL110839. https://doi.org/10.1029/2024GL110839

Received 14 JUN 2024
Accepted 22 AUG 2024

Author Contributions:

Data curation: Savvas Raptis
Formal analysis: Savvas Raptis, Viacheslav Merkin, Shinichi Ohtani, Matina Gkioulidou
Funding acquisition: Viacheslav Merkin
Investigation: Savvas Raptis, Viacheslav Merkin, Shinichi Ohtani, Matina Gkioulidou
Methodology: Savvas Raptis, Viacheslav Merkin, Shinichi Ohtani, Matina Gkioulidou
Project administration: Viacheslav Merkin
Software: Savvas Raptis
Supervision: Viacheslav Merkin
Visualization: Savvas Raptis
Writing – original draft: Savvas Raptis

Abstract Plasma sheet convection is a key element of storm-time plasma dynamics in the magnetosphere. While decades of observations have advanced our understanding of convection in general, specifically storm-time convection remains poorly understood. Using data from ISAS/NASA's Geotail and NASA's MMS, this study characterizes plasma sheet magnetic flux transport across the magnetotail during numerous storms (both recovery and main phases) and contrasts these observations with those from quiet times. Our findings confirm the well-documented enhancement of the convection electric field during geomagnetic storms. Beyond that, our results reveal a significant dawn-dusk asymmetry. At dawn, the elevated convection is realized via relatively faster flows while at dusk, through a stronger northward magnetic field. These findings suggest a complex feedback loop between plasma sheet convection and ring current buildup, whereby the latter asymmetrically inflates the magnetotail on the dusk side, shifting the reconnection site and subsequently enhanced earthward flows toward dawn.

Plain Language Summary Strong solar activity creates major disruptions of the Earth's magnetic field known as geomagnetic storms. These major disturbances of near-Earth space can impact essential technologies like GPS systems and power grids. Our research used data from two space missions, ISAS/NASA's Geotail and NASA's MMS, to study how particles and magnetic fields move in space around Earth during such storms. We compared storm periods to calm times and evaluated the differences. During geomagnetic storms, we found that charged particles transport more magnetic flux due to stronger electric field. We further noted a significant difference between the dawn (morning) and dusk (evening) sectors on the nightside of the near-Earth space environment. During storm times, plasma moves faster on the dawn side, while the magnetic field is stronger on the dusk side. This discovery reveals that plasma movement and energy buildup during storms are more complex than we thought. The energy buildup on the dusk side pushes plasma movement more toward the dawn side. Understanding these details helps us better predict the impacts of geomagnetic storms on Earth's space environment, which can improve our ability to protect our technology and infrastructure.

1. Introduction

Geomagnetic storms are major disturbances of the magnetosphere-ionosphere-thermosphere system. Storms are driven by solar coronal mass ejections (CMEs) or high-speed solar wind streams, and are characterized by ring current buildup and a global reconfiguration of the geomagnetic field. These explosive phenomena are typically accompanied by heightened magnetospheric convection, especially pronounced during the main phase of a storm when the magnetospheric system responds to strong solar wind driving (Gonzalez et al., 1994; Lakhina & Tsurutani, 2016; Tsyganenko et al., 2003). Convection plays a crucial role in storm dynamics by facilitating the return of the magnetic flux to the dayside and driving plasma toward Earth, thereby enhancing the ring current.

While it is well-established that nightside plasma sheet convection significantly influences the ring current, the specifics of this process at various spatial and temporal scales remain unclear. Nightside convection, irrespective of storm activity, is linked to bursty intervals of elevated velocity associated with magnetic flux transport, known as bursty bulk flows (BBFs) (Angelopoulos et al., 1992, 1994; Baumjohann et al., 1990; Runov et al., 2011). These transient phenomena are vital for transferring energy flux and plasma from the magnetotail to the inner magnetosphere, contributing to the ring current buildup and making the magnetotail more dipolar (Birn et al., 2019; Merkin et al., 2019; Sciola et al., 2023; Yang et al., 2015). On the other hand, during storm times, global-scale convection can contribute significantly to the ring current enhancement (Daglis, 2006; Daglis et al., 1999; Kamide et al., 1998).

Writing – review & editing:
Viacheslav Merkin, Shinichi Ohtani, Matina Gkioulidou, Leonardo H. Regoli

Currently, our understanding of nightside convection during storms is limited. While the average plasma sheet convection is relatively well documented (Baumjohann et al., 1989; Borovsky et al., 1998; Juusola et al., 2011; Kaufmann & Paterson, 2006; Wolf et al., 2009), little research has addressed storm-time behavior and distinguished it from quiet-time activity (Hori et al., 2005; Ohtani & Mukai, 2008). In particular, while spatial asymmetries between dusk and dawn magnetosphere have been observed and discussed for decades very limited work can be found addressing storm times regarding that matter (Haaland et al., 2017). However, due to recent advancements in examining the asymmetric configuration of the partial ring current (PRC) (Ebihara et al., 2002; Ohtani, 2021), one would expect that plasma sheet properties should statistically experience an associated asymmetry.

This letter aims to explore plasma sheet dynamics during geomagnetic storms using multi-spacecraft measurements and statistical analysis. Specifically, we investigate the variability of plasma sheet magnetic flux transport during 'quiet' periods and times of geomagnetic activity (main and recovery storm phase). We primarily use data from the ISAS/NASA Geotail mission (01/1994–12/2022) (Nishida, 1994) and supplement our findings with measurements from the NASA Magnetosphere Multiscale (MMS) mission (09/2015–01/2024) (Burch et al., 2016). First, we analyze the spatial distribution of various parameters characterizing plasma sheet convection, namely, the convection electric field, the bulk flow perpendicular to the magnetic field, and the equatorial magnetic field across the magnetotail. To that end, we present how these quantities vary along the Sun-Earth line. Then we proceed by showing how this variability changes between the dusk and dawn sector, giving rise to an intriguing asymmetry. In the last section, we discuss the interpretation and implications of these findings for understanding plasma sheet convection during geomagnetic storms. In particular, we discuss how our results compare with recent findings and interpretation of the ring current configuration and how transient events like BBFs can be incorporated in this framework in the future.

2. Method

2.1. Data

For the analysis, we use Geocentric Solar Magnetospheric (GSM) coordinates aberrated by 4°. The whole available Geotail data set is used, ranging from −10 Earth radii (R_E) to −31 for $X_{GSM,4°}$, and from −10 to +10 R_E for $Y_{GSM,4°}$. The Geotail measurements were collected over the period for which data are available (1994–2022) having a resolution of 12 s. The magnetic field measurements are obtained through the magnetic field experiment (MGF) instrument (Kokubun et al., 1994) while the ion plasma moments are from the low-energy plasma experiment (LEP) (Mukai et al., 1994). The details of this data set and its utilization are extensively described by Nagai et al. (2023). For part of the analysis we used MMS measurements. Due to the proximity of the satellites, only data from the first spacecraft (MMS1) were included, as MMS2-4 data were identical for the spatial and temporal scales examined in this study. Plasma moments were derived from the Hot Plasma Composition Analyzer (HPCA) (Young et al., 2016) which has an average time resolution of 15 s in survey mode. HPCA measures ion flux within an energy range of $K/q \in [0.01 - -40\mathrm{keV/q}]$. In our work we focused on H^+ ions, the dominant species in the plasma sheet region. Magnetic field measurements were obtained from the fluxgate magnetometer (FGM) (Russell et al., 2016) with a survey mode resolution of 16 Hz. However, the FGM data were resampled/averaged to match the temporal resolution of HPCA measurements. The choice of HPCA over the Fast Plasma Investigation (FPI) ion instrument (Pollock et al., 2016) was based on two factors: (a) its intrinsic time resolution, which is more similar to that of the Geotail instrument, facilitating less biased comparisons, and (b) the potential presence of instrumental variations due to the differing energy limits between FPI and LEP. It should be noted however, that preliminary results with the FPI instrument produced similar results to the HPCA. The MMS data used in this study cover the period from September 2015 to January 2024. For quantifying the convection electric field we are using $(-\mathbf{V}\times\mathbf{B})_y$ which is ideal for statistical studies since it is well correlated to the measured E_y, and available for the whole Geotail mission (Kasaba et al., 2006; Ohtani & Mukai, 2008). More information regarding the different electric field quantities can be found in the supplementary material. Finally, to associate the *in-situ* observations with storm activity, we utilized the SuperMAG ring current index (SMR) which is equivalent to the Sym-H index. SMR is an average index based on all available ground stations located between −50 and +50 magnetic latitude (MLat) (Newell & Gjerloev, 2012).

2.2. Geomagnetic Storm Characterization

We define a geomagnetic storm as an interval marked by ring current intensification, inferred from ground magnetic field depletion and quantified by the SMR index. Specifically, we classify an interval as a storm if the SMR index drops to −50 nT or less. Additionally, we determine the start and end of the storm by identifying the times when the SMR index reaches −10 nT before and after its minimum value. To make sure we include sufficient measurements to capture the full main and recovery phase, we introduce 2h margin before and after the first time and last time −10 nT is reached respectively. After compiling a list of storms, we identify the recovery and main phases by using a peak finder algorithm as compiled by Python's *scipy* "signal.find_peaks" function. The algorithm's reliability was confirmed by validating with the 2003 Halloween storm. Comparing with the methodology outlined in Ohtani (2021), our classification yielded similar results. The list of storms and associated phase (recovery and main) characterization is provided in the Open Research statement below. In all figures presented, the various characterizations based on geomagnetic storm activity are color-coded as follows: quiet periods (black), recovery phase (blue), and main phase (red). We should clarify that quiet periods are equivalent to non-storm periods. Further distinction, such as in terms of substorm activity is out of the scope of this work.

2.3. Plasma Sheet Classification

The classification of the central plasma sheet and its distinction from nearby regions (i.e., lobes, boundary layer, and magnetosheath) is challenging (Grigorenko et al., 2012). Typically, this is addressed by applying a set of criteria based on plasma beta and/or equatorial magnetic field (B_z). Other approaches may utilize thresholds on ion density, temperature, or specific entropy (e.g., Borovsky et al., 1998; Burin des Roziers et al., 2009; Guild et al., 2008; Ohtani & Mukai, 2008; Vo et al., 2023). These criteria are highly dependent on instrumental capabilities and may not be easily transferable between missions. However, by employing relatively strict criteria, one can minimize false positive intervals regardless of the mission, instrument used, or presence of variable external drivers. In our study, we adopted criteria similar to the one described by Burin des Roziers et al. (2009), which is comparable to the one used by Ohtani and Mukai (2008), while somewhat less restrictive. Specifically, the spacecraft needs to be within $\pm 10 R_E$ in $Y_{GSM,4^\circ}$ and $Z_{GSM,4^\circ}$ and from −5 to −31 R_E in $X_{GSM,4^\circ}$. Additionally, we required that the equatorial magnetic field B_z exceeds the B_{xy} component through the condition $|B_z| > \frac{1}{2}\sqrt{B_x^2 + B_y^2}$. To exclude lobe measurements, we imposed that the plasma beta, as computed from ion moments, must be greater than unity $(\beta_i > 1)$. To further minimize false positive measurements, we added a criterion that the ion density must satisfy $n_i < 4$ [1/cc] for both Geotail and MMS measurements (corresponding to $>99\%/3\sigma$ of the statistical sample). This additional criterion removes data points corresponding to nightside magnetosheath. Furthermore, for the Geotail data we use the EA (Energy Analyzer) mode, which provides the optimal data set for magnetospheric studies. This relatively strict set of criteria ensure that measurements are taken near the central plasma sheet region. It is important to note that the bulk properties of the plasma sheet obtained from either MMS or Geotail data can vary by up to ∼10%, depending on the criteria or thresholds applied. This implies that the results presented below are robust when considered as relative differences between different geomagnetic activity states (quiet, recovery, and main phase). However, the absolute values may be influenced by instrumental effects, orbital biases, and selection criteria, and therefore should be interpreted with caution. The final data sample produced by the above methodology, encompassing storm characterization and associated plasma sheet measurements for both missions, can be visualized in Figure 1. As shown there, the number of data points during the main phase is considerably smaller than during the recovery phase, which in turn is an order of magnitude lower compared to quiet times.

3. Results

Ohtani and Mukai (2008) showed that during storm times there is an elevated convection electric field, $(-\mathbf{V} \times \mathbf{B})_y$. This enhancement correlated with a more dipolar (B_z) magnetic field and minimal changes in earthward flow perpendicular to the magnetic field ($V_{\perp,x}$). We have qualitatively confirmed these findings using both the latest extensive Geotail data set and MMS. Although, as shown below, variations exist due to different instrumentation and data processing, the shape of the distributions and the relative differences appear consistent, supporting previous results. Having established the validity of our data set, Figure 2 illustrates the distribution of the convection electric field (E_y), B_z and $V_{\perp,x}$ along the $X_{GSM,4^\circ}$ axis from close to Earth ($-5R_E$) to the outer tail ($-31R_E$). Table S1

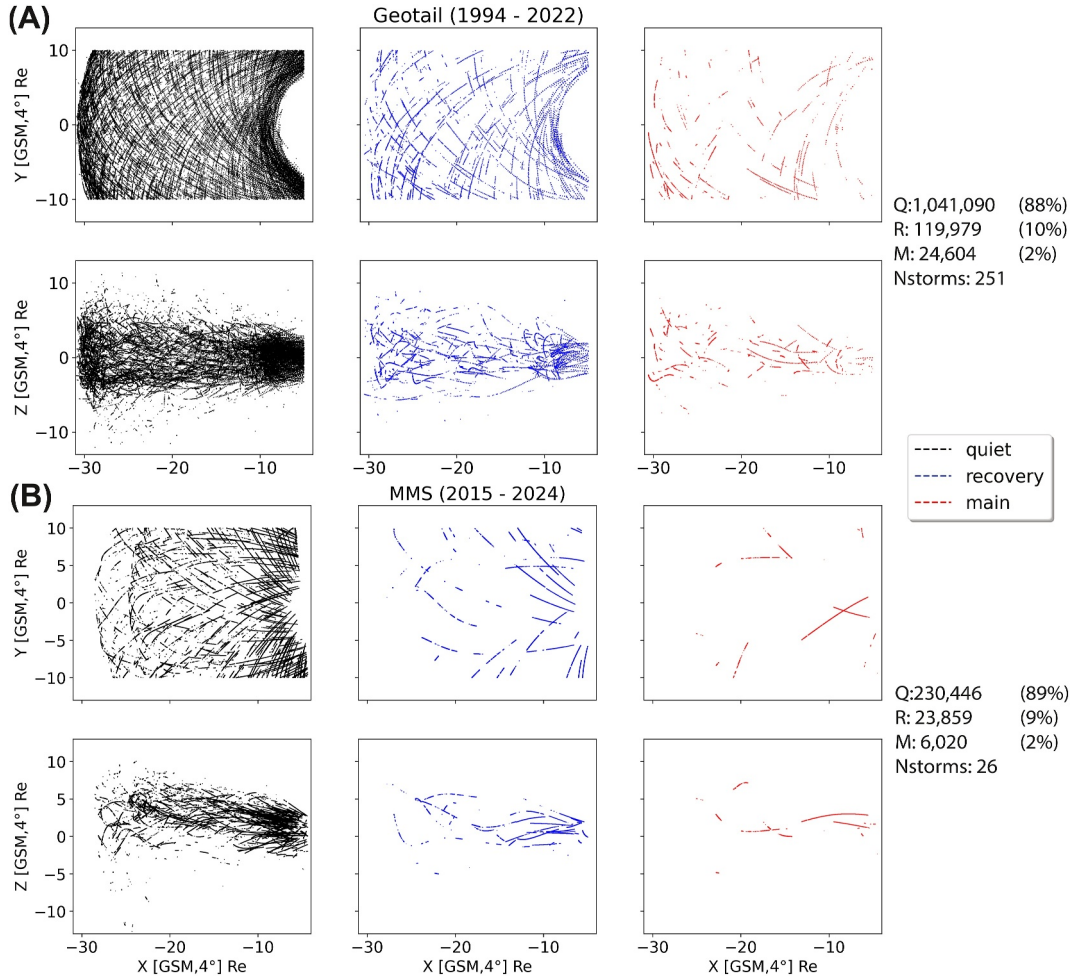

Figure 1. Plasma sheet observations during quiet times (black), recovery phase (blue), and main phase (red) in XY and XZ Geocentric Solar Magnetospheric (GSM) coordinates aberrated by 4°. Each panel consists of a scatter plot with each point being a single measurement for (a) Geotail measurements from 1994 to 2022, and for (b) MMS data from 2015 to 2024. On the right of each subplot the number of storms, along with the number of measurements per phase and its percentage with respect to the full data set is shown. Due to different periods and orbits between the missions, there is approximately an order of magnitude difference between the number of data points and storms.

in Supporting Information S1 presents statistical confidence details for each point shown in the plot. As shown in Table S1 in Supporting Information S1, MMS data are notably less robust for this analysis due to the low number of storm intervals contained in the data set. Figure 2 demonstrates that the enhancement of the convection electric field during storm times spans the entire magnetotail. Additionally, this enhancement correlates with a consistent increase in the northward magnetic field throughout all spatial bin for the recovery and even more prominently for the main storm phase. However, both Geotail (Figure 2b) and MMS (Figure 2e) observations show elevated $V_{\perp,x}$ primarily during the main phase of the storm at the outer magnetosphere ($X < -20R_E$) and at the inner ($X > -15R_E$) part. This trend is more noticeable in Geotail measurements. Notably, the relative differences are most pronounced at the 75th percentile of the distribution, suggesting the presence of faster flows in the tail of the distribution during the main storm phase. Qualitatively, the changes in the bulk flow along the tail appear to be associated with localized peaks/dips in the distribution of the convection electric field, while the overall relative increase (i.e., distribution shape) compared to quiet times arises primarily from the elevation of B_z. While it is difficult to quantify the exact contribution, the dip observed at Figure 2a, at about $-15R_E$ and the peaks at about $-28R_E$ and $-7R_E$ are co-located with the ones observed in Figure 2b. The overall elevation, however (consistent increase across all spatial bins) appears to correlate better with the trends shown on Figure 2c. At this point we should stress that the limited number of storms and the data samples available for MMS (Figure 1) preclude any

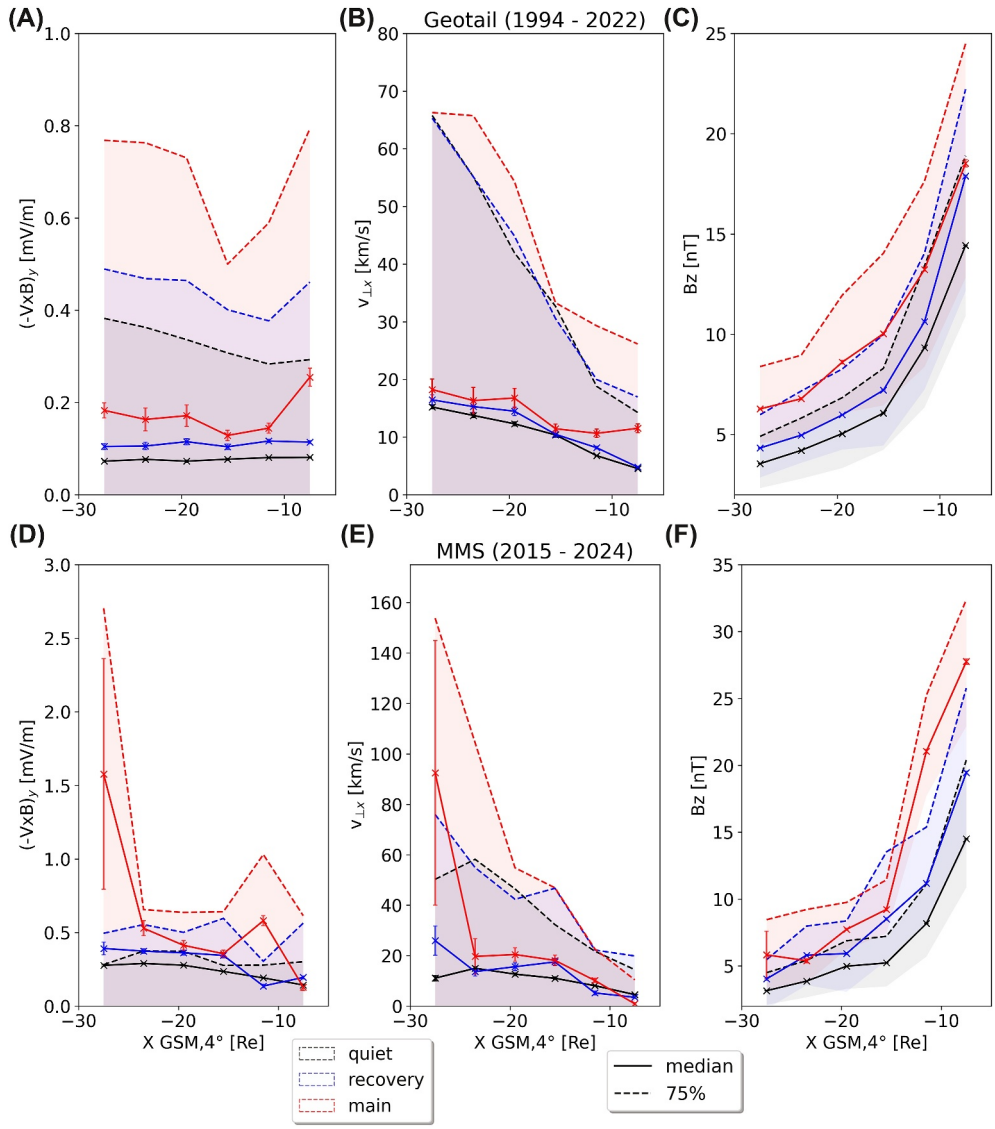

Figure 2. Spatial distributions along $X_{GSM,4°}$ of (a) $(-\mathbf{V}\times\mathbf{B})_y$ (b) $V_{\perp,x}$, and (c) B_z for Geotail measurements. Panels d–f show the same quantities but for MMS. The solid lines indicate the median values for each quantity, while the dotted ones and the shaded area describe the 75th percentiles of the distribution. For completeness, shaded area includes 25th percentiles for panels (c) and (f). The error bars for each data point represent the standard error (SE), calculated as $SE = SD/\sqrt{N}$, where SD is the standard deviation and N is the number of data points per bin. Similar to the rest of the text, black color denotes quiet times, blue the recovery phase, and red the main storm phase. The bins along the $X_{GSM,4°}$ axis used to generate all subplots are [(−5, −10) (−9, −14) (−13, −18) (−17, −22) (−21, −26) (−25, −30)]. More details on the statistical metrics of this figure are given in the supplementary material (see Table S1 in Supporting Information S1).

statistical robustness in the following part of the analysis. This limitation arises because the binning in the XY GSM plane, particularly during the main phase of a storm, drastically reduces the number of data points, rendering further use of MMS data impractical. Additional information, along with precise figures, can be found in the supplementary material (refer to Table S1–S2 in Supporting Information S1 and the associated discussion). Moving on, to investigate further the storm time plasma sheet convection, we explored the same physical quantities, as they appear in the XY GSM plane. Given the similarities between the differences observed during the recovery and main phases compared to quiet periods (Figure 2), we show here only the main phase statistics normalized relative to the quiet phase in Figure 3 (i.e., $\Delta Q = Q_{main} - Q_{quiet}$ per spatial bin). The original data from which Figure 3 is derived can be found in the supplementary material (Figure S1–S3 in Supporting Information S1) and are further discussed on the discussion section below. Evaluating Figure 3a, two notable effects emerge. First, in comparison with the study by

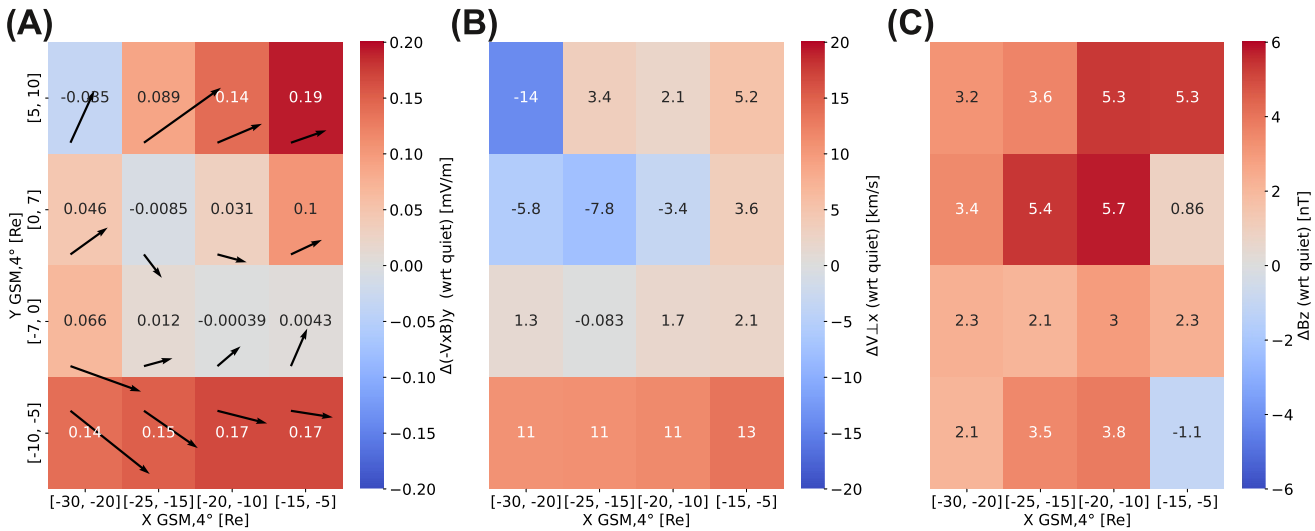

Figure 3. 2D histograms using Geotail measurements within the plasma sheet. The *X* axis indicates the binning along $X_{GSM,4°}$ while the *Y* axis along $Y_{GSM,4°}$. (a) Shows the median difference of the convection electric field, $(-\mathbf{V}\times\mathbf{B})_y$, between the main storm phase and quiet time. The arrows show the median direction of the plasma flow during the main storm phase (similar results are obtained when using $\mathbf{V}_\perp$). (b) Indicates the earthward perpendicular to the magnetic field velocity ($V_{\perp,x}$), again relative to quiet time. (c) Shows the difference in the equatorial magnetic field (B_z) between main phase and quiet periods. The text in each box is the median value represented by the color bar, on the right of each subplot. More details on the statistical metrics of this figure are given in the supplementary material (see Table S2 in Supporting Information S1).

Nagai et al. (2023, Figure 19), which averaged Geotail plasma sheet measurements over all types of activity, it becomes apparent that during the main phase of a storm, which is the focus of our study, plasma flows become more irregular, while, as expected, remaining faster further from Earth. Additionally, the relative increase in the convection electric field (compared to quiet time) appears to cluster in the dawn and inner dusk sectors, a novel observation not captured when integrating along the *y*-axis (Figure 2). Figure 3b indicates that the elevation of E_y in the dawn-side magnetotail (Figure 3a) is realized through an enhancement of $V_{\perp,x}$ a trend notably absent in the dusk sector, particularly in the outer tail where, during the main phase, flows statistically tend to be less Earthward. Lastly, Figure 3c indicates that the increase in E_y at the dusk is predominantly linked to an elevated dipolar field (B_z), evident across multiple spatial locations. It is important to note that while median values are presented in both Figures 2 and 3, similar asymmetries, relative differences and trends were observed in average/mean values and 0.75 quantiles, albeit with different absolute values. Finally, since we are concentrating on earthward magnetic flux transport, to further validate our results, we excluded tailward reconnection outflow from the data set by removing data points that had $B_z < 0$ and $V_x < 0$. As these points are a tiny fraction of the data set (<1%) the statistical picture remained virtually the same.

4. Discussion

In this study, we conducted a comprehensive characterization of magnetotail plasma sheet convection during periods of storm activity (main and recovery phases) juxtaposed with quiet time. Leveraging the extensive data set from Geotail and state-of-the-art measurements from MMS, we observed a systematic and significant elevation in the storm-time convection electric field (E_y) across the magnetotail, spanning from −5 to −30 R_E. This enhancement manifests through a profound asymmetry: the dusk sector is associated with a more dipolar magnetic field (enhanced B_z), while the dawn magnetotail is characterized by relatively faster earthward flows perpendicular to the magnetic field ($V_{\perp,x}$). Notably, this storm-time asymmetry has not been statistically observed using *in-situ* measurements before, though data-based modeling during geomagnetic storms has shown a stronger B_z in the dusk sector (Sitnov et al., 2008, Figure 10). These findings provide validation to our observations and support these modeling efforts. Before interpreting this result we need to evaluate a potential limitation of our approach, possibly influencing previous efforts as well (Hori et al., 2005; Ohtani & Mukai, 2008). The question is whether there is an observational bias caused by a correlation between the strength of the storm and the spacecraft dawn/dusk location. After evaluating Geotail data obtained during main phases,

we found that the average SMR depletion was about −48 nT when the spacecraft was in the dusk sector while it was −33 nT when the spacecraft was in the dawn sector. The minimum and median SMR along with the recovery phase behavior showed similar differences. This relatively small difference along with a very weak correlation (r) between B_z and SMR ($r_{dawn} \approx -0.25$ and $r_{dusk} \approx -0.15$, $p < 0.001$) increases the certainty of our results. However, in future work an approach that allows the severity of the storm to be incorporated in the analysis would be beneficial to fully eliminate any potential bias of this type. Another, caveat which applies to all *in-situ* data analysis is the instrumentation uncertainties involved. Since our work compares statistical distributions, the instrumental error averages out, allowing a statistically significant result in relative terms (i.e., comparing stormtime to non-stortime plasmasheet) to emerge. However, due to instrumental errors a direct quantification of the field and its difference is not achievable by our methodology. Such quantification may be unobtainable as the absolute number of a quantity relies strongly on the calibration of each instrument and can vary between missions. Recent findings offer promising avenues for interpreting the observed asymmetries in storm-time magnetotail convection. Our observations align with the concept of the dawnside current wedge (DCW), which was recently formulated and exemplified via observations by Ohtani (2021). Essentially, DCW is similar to the substorm current wedge but it is specifically a storm-time phenomenon occurring on the dawn side of the magnetosphere. Sorathia et al. (2023) demonstrated that such a current system can also arise in simulations of geomagnetic storms. One interpretation of the DCW is that during storms, the presence of the pre-midnight ring current peak causes an elevated B_z in the dusk sector tail, that is, the tail becomes ”inflated”, potentially suppressing reconnection there and shifting its statistical occurrence toward the dawn sector, where B_z is lower. Consequently, reconnection outflows are predominantly observed at dawn (Figure 3b). As the tail returns to quiet values during the recovery phase, this effect diminishes. Elevated flows contributing to enhanced convection and subsequent magnetic field dipolarization in the dawn-side inner magnetosphere eventually mitigate the asymmetry, leading to a more symmetric configuration typically found during quiet times. Our findings support this picture. An alternative explanation of the observed flow asymmetry is that the faster flow at dawn originates from fast flows originally formed at pre-midnight but deflected dawn-ward due to the elevated dusk-side magnetic field (Zhou et al., 2014). However, the absence of elevated midnight flows and the overall observed flow patterns do not support this scenario. While our results qualitatively align with the above interpretation of the DCW, they also suggest a more complex scenario (e.g., relative elevation of faster flow along both dusk and dawn flanks). Another question arises if we compare our results with the work of Sorathia et al. (2023). Specifically, the relatively lower dipolarization at the dawn compared to the dusk in the inner part of the magnetotail found in our work might appear to be at variance with Figure 6 in their paper. However, this seeming disagreement may originate from the fact that in our case the inner-most bin in Figure 3 averages the data within $X \in [-15, -5]$ R_E) for many events, whereas Sorathia et al. (2023, Figure 6) focuses on the evolution of one storm at a fixed radial distance of 6 R_E, which is at the very edge of our statistical binning. It is possible that the dawnside dipolarization during the main phase shown by Sorathia et al. (2023) is too close to Earth to be picked up by our statistics. Furthermore, as we discuss below, different quantities (and their asymmetries) evolve on different time scales which affects their statistical properties. Finally, it is important to note that the analyses presented in Figures 2 and 3 and the supplementary material represent median statistical behavior. Therefore, the possible presence and effect of fast flows (e.g., BBFs) remains unknown, necessitating more detailed analysis to assess their contribution. Our results indicate that the behavior of plasma sheet convection during the main and recovery phases of a storm follows similar trends. While the convective field during the recovery phase is relatively lower compared to the main phase (Figure 2 and supplementary material), it remains consistently elevated throughout the magnetotail (relative to quiet times). Interestingly, when examining the dawn/dusk asymmetry, similarities remain apparent in the convection electric field and equatorial magnetic field regardless of whether the storm is undergoing its main or recovery phase (Figures 2a and 2d and Figures S2, S4 in Supporting Information S1). However, the observed asymmetry in the flows is not present for the recovery phase (Figure S3 in Supporting Information S1). This suggests that the elevated northward magnetic field in the dusk magnetotail is an overall characteristic of the storm-time plasma sheet, while the enhanced dawnside $V_{\perp,x}$ is a feature exclusive to the storm's main phase. This result implies that the relaxation of the magnetic field as the plasma sheet configuration returns to quiet-time values takes longer compared to the unwinding of the elevated dawnside flow. Nagai et al. (2023) showed that reconnection during intense solar wind conditions occurs more frequently in the midnight and dawn sectors (compared to quiet times), while weak driving allows magnetotail reconnection to occur more toward dusk. During a prolonged recovery phase, the solar wind driving is statistically weaker, which allows magnetotail reconnection to return to its nominal location, rapidly eliminating the presence of faster flows

at the dawn side. This picture is further supported by the fact that under intense solar wind, current sheet thinning and reconnection outflows occur on faster time scales than during weak driving (Nagai et al., 2023; Nagai & Shinohara, 2021; Pitkänen et al., 2021). Furthermore, when the solar wind driving changes, the corresponding plasma sheet field reconfiguration occurs first in the far magnetotail and later in the near-Earth plasma sheet (Borovsky et al., 1998; Wing et al., 2014). This can create a mismatch between the observed asymmetries as the storm transitions from the main to the recovery phase and finally to quiet time, with the $V_{\perp,x}$ asymmetry rapidly dissolving and the B_z fading more gradually. Finally, our findings suggest that statistically enhanced earthward flows, with the exception of the dusk sector, are more prominent during storm activity compared to quiet times. However, examining the tail of the distribution (75th percentile of Figures 2b and 2e) reveals an enhancement that corresponds to the localized behavior observed in the convection electric field (Figures 3a and 3d). This suggests that the enhancement of B_z between quiet and storm times plays a significant role in shaping plasma sheet dynamics. However, the presence of fast flows in the tail of the velocity distribution may be associated with localized peaks in the convection electric field, $(-\mathbf{V}\times\mathbf{B})_y$. While our work was focused on the "frozen-in" behavior of bulk plasma characteristic of magnetized protons, it is important to recognize that during storm times, there is a significant population of heavier ions such as O+ and He+ (Kronberg et al., 2014; Ohtani et al., 2011; Regoli et al., 2024). These ions can impact the characterization of all plasma moments, which was not considered in the analysis of either Geotail or MMS measurements. Evaluating the different ion species and their effects on the convection electric field using MMS measurements would be beneficial for fully characterizing plasma convection, but will be statistically limited due to insufficient number of measurements at this time, as discussed above. Finally, another key point to investigate in the future is whether plasma sheet convection and its observed asymmetries vary between the storms that are driven by CMEs compared to these driven by Stream interaction regions (SIRs) since they have very different solar wind driving and subsequent plasma sheet properties (Andreeva & Tsyganenko, 2019; Borovsky & Denton, 2006; Stephens et al., 2013).

Data Availability Statement

Geotail data are available through https://darts.isas.jaxa.jp/stp/geotail/data.html. Magnetospheric Multiscale (MMS) measurements can be found through https://lasp.colorado.edu/mms/sdc/public/about/browse-wrapper/ or through the Graphical User Interface (GUI) found in https://lasp.colorado.edu/mms/sdc/public/search/. The SuperMAG indices are available via https://supermag.jhuapl.edu. We acknowledge the use of irfu-matlab package, https://github.com/irfu/irfu-matlab, and pySPEDAS https://pyspedas.readthedocs.io/en/latest/. The list of all geomagnetic storms classified in main and recovery phase from 1993 to 2023 can be accessed through the associated Zenodo data set (Raptis, 2024).

Acknowledgments
This research was supported by the NASA DRIVE Science Center for Geospace Storms (CGS) under award 80NSSC22M0163. SO acknowledges support by NSF under award 2224986, and NASA under award 80NSSC21K0036. VGM acknowledges support by NASA under award 80NSSC23K0223. SR acknowledges support by the Magnetospheric Multiscale (MMS) mission of NASA's Science Directorate Heliophysics Division via subcontract to the Southwest Research Institute (NNG04EB99C). SR thanks Louis Richard for the useful discussions and Tsugunobu Nagai for their valuable input and feedback on our work along with assistance in obtaining and processing the Geotail data set.

References

Andreeva, V., & Tsyganenko, N. (2019). Empirical modeling of the geomagnetosphere for sir and cme-driven magnetic storms. *Journal of Geophysical Research: Space Physics*, *124*(7), 5641–5662. https://doi.org/10.1029/2018ja026008

Angelopoulos, V., Baumjohann, W., Kennel, C., Coroniti, F. V., Kivelson, M., Pellat, R., et al. (1992). Bursty bulk flows in the inner central plasma sheet. *Journal of Geophysical Research*, *97*(A4), 4027–4039. https://doi.org/10.1029/91ja02701

Angelopoulos, V., Kennel, C., Coroniti, F., Pellat, R., Kivelson, M., Walker, R., et al. (1994). Statistical characteristics of bursty bulk flow events. *Journal of Geophysical Research*, *99*(A11), 21257–21280. https://doi.org/10.1029/94ja01263

Baumjohann, W., Paschmann, G., & Cattell, C. (1989). Average plasma properties in the central plasma sheet. *Journal of Geophysical Research*, *94*(A6), 6597–6606.

Baumjohann, W., Paschmann, G., & Lühr, H. (1990). Characteristics of high-speed ion flows in the plasma sheet. *Journal of Geophysical Research*, *95*(A4), 3801–3809.

Birn, J., Liu, J., Runov, A., Kepko, L., & Angelopoulos, V. (2019). On the contribution of dipolarizing flux bundles to the substorm current wedge and to flux and energy transport. *Journal of Geophysical Research: Space Physics*, *124*(7), 5408–5420. https://doi.org/10.1029/2019ja026658

Borovsky, J. E., & Denton, M. H. (2006). Differences between cme-driven storms and cir-driven storms. *Journal of Geophysical Research*, *111*(A7). https://doi.org/10.1029/2005ja011447

Borovsky, J. E., Thomsen, M. F., & Elphic, R. C. (1998). The driving of the plasma sheet by the solar wind. *Journal of Geophysical Research*, *103*(A8), 17617–17639. https://doi.org/10.1029/97ja02986

Burch, J., Moore, T., Torbert, R., & Giles, B.-h. (2016). Magnetospheric multiscale overview and science objectives. *Space Science Reviews*, *199*(1–4), 5–21. https://doi.org/10.1007/s11214-015-0164-9

Burin des Roziers, E., Li, X., Baker, D., Fritz, T., Friedel, R., Onsager, T., & Dandouras, I. (2009). Energetic plasma sheet electrons and their relationship with the solar wind: A cluster and geotail study. *Journal of Geophysical Research*, *114*(A2). https://doi.org/10.1029/2008ja013696

Daglis, I. A. (2006). Ring current dynamics. *Space Science Reviews*, *124*, 183–202. https://doi.org/10.1007/978-0-387-69532-7_13

Daglis, I. A., Thorne, R. M., Baumjohann, W., & Orsini, S. (1999). The terrestrial ring current: Origin, formation, and decay. *Reviews of Geophysics*, *37*(4), 407–438. https://doi.org/10.1029/1999rg900009

Ebihara, Y., Ejiri, M., Nilsson, H., Sandahl, I., Milillo, A., Grande, M., et al. (2002). Statistical distribution of the storm-time proton ring current: Polar measurements. *Geophysical Research Letters*, *29*(20), 30–31. https://doi.org/10.1029/2002gl015430

Gonzalez, W., Joselyn, J.-A., Kamide, Y., Kroehl, H. W., Rostoker, G., Tsurutani, B. T., & Vasyliunas, V. (1994). What is a geomagnetic storm? *Journal of Geophysical Research*, *99*(A4), 5771–5792. https://doi.org/10.1029/93ja02867

Grigorenko, E. E., Koleva, R., & Sauvaud, J.-A. (2012). On the problem of plasma sheet boundary layer identification from plasma moments in earth's magnetotail. *Annales Geophysicae*, *30*(9), 1331–1343. https://doi.org/10.5194/angeo-30-1331-2012

Guild, T. B., Spence, H. E., Kepko, E. L., Merkin, V., Lyon, J. G., Wiltberger, M., & Goodrich, C. C. (2008). Geotail and lfm comparisons of plasma sheet climatology: 1. Average values. *Journal of Geophysical Research*, *113*(A4). https://doi.org/10.1029/2007ja012611

Haaland, S., Runov, A., & Forsyth, C. (2017). *Dawn-dusk asymmetries in planetary plasma environments* (Vol. 230). John Wiley and Sons.

Hori, T., Lui, A., Ohtani, S. C., Maezawa, K., Mukai, T., Kasaba, Y., et al. (2005). Storm-time convection electric field in the near-earth plasma sheet. *Journal of Geophysical Research*, *110*(A4). https://doi.org/10.1029/2004ja010449

Juusola, L., Østgaard, N., & Tanskanen, E. (2011). Statistics of plasma sheet convection. *Journal of Geophysical Research*, *116*(A8). https://doi.org/10.1029/2011ja016479

Kamide, Y., Baumjohann, W., Daglis, I., Gonzalez, W., Grande, M., Joselyn, J., et al. (1998). Current understanding of magnetic storms: Storm-substorm relationships. *Journal of Geophysical Research*, *103*(A8), 17705–17728. https://doi.org/10.1029/98ja01426

Kasaba, Y., Hayakawa, H., Ishisaka, K., Okada, T., Matsuoka, A., Mukai, T., & Takei, Y. (2006). Evaluation of dc electric field measurement by the double probe system aboard the geotail spacecraft. *Advances in Space Research*, *37*(3), 604–609. https://doi.org/10.1016/j.asr.2005.05.006

Kaufmann, R. L., & Paterson, W. R. (2006). Magnetic flux and particle transport in the plasma sheet. *Journal of Geophysical Research*, *111*(A10). https://doi.org/10.1029/2006ja011734

Kokubun, S., Yamamoto, T., Acuña, M. H., Hayashi, K., Shiokawa, K., & Kawano, H. (1994). The geotail magnetic field experiment. *Journal of Geomagnetism and Geoelectricity*, *46*(1), 7–21. https://doi.org/10.5636/jgg.46.7

Kronberg, E. A., Ashour-Abdalla, M., Dandouras, I., Delcourt, D. C., Grigorenko, E. E., Kistler, L. M., et al. (2014). Circulation of heavy ions and their dynamical effects in the magnetosphere: Recent observations and models. *Space Science Reviews*, *184*(1–4), 173–235. https://doi.org/10.1007/s11214-014-0104-0

Lakhina, G. S., & Tsurutani, B. T. (2016). Geomagnetic storms: Historical perspective to modern view. *Geoscience Letters*, *3*, 1–11. https://doi.org/10.1186/s40562-016-0037-4

Merkin, V. G., Panov, E. V., Sorathia, K., & Ukhorskiy, A. Y. (2019). Contribution of bursty bulk flows to the global dipolarization of the magnetotail during an isolated substorm. *Journal of Geophysical Research: Space Physics*, *124*(11), 8647–8668. https://doi.org/10.1029/2019ja026872

Mukai, T., Machida, S., Saito, Y., Hirahara, M., Terasawa, T., Kaya, N., et al. (1994). The low energy particle (lep) experiment onboard the geotail satellite. *Journal of Geomagnetism and Geoelectricity*, *46*(8), 669–692. https://doi.org/10.5636/jgg.46.669

Nagai, T., & Shinohara, I. (2021). Dawn-dusk confinement of magnetic reconnection site in the near-earth magnetotail and its implication for dipolarization and substorm current system. *Journal of Geophysical Research: Space Physics*, *126*(11), e2021JA029691. https://doi.org/10.1029/2021ja029691

Nagai, T., Shinohara, I., Saito, Y., Ieda, A., & Nakamura, R. (2023). Location and timing of magnetic reconnections in earth's magnetotail: Accomplishments of the 29-year geotail near-earth magnetotail survey. *Journal of Geophysical Research: Space Physics*, *128*(12), e2023JA032023. https://doi.org/10.1029/2023ja032023

Newell, P., & Gjerloev, J. (2012). Supermag-based partial ring current indices. *Journal of Geophysical Research*, *117*(A5). https://doi.org/10.1029/2012ja017586

Nishida, A. (1994). The geotail mission. *Geophysical Research Letters*, *21*(25), 2871–2873. Retrieved from https://agupubs.onlinelibrary.wiley.com/doi/abs/10.1029/94GL01223doi:10.1029/94GL01223

Ohtani, S. (2021). Revisiting the partial ring current model: Longitudinal asymmetry of ground magnetic depression during geomagnetic storms. *Journal of Geophysical Research: Space Physics*, *126*(9), e2021JA029643. https://doi.org/10.1029/2021ja029643

Ohtani, S., & Mukai, T. (2008). Statistical characteristics of the storm time plasma sheet. *Journal of Geophysical Research*, *113*(A1). https://doi.org/10.1029/2007ja012547

Ohtani, S., Nosé, M., Christon, S., & Lui, A. (2011). Energetic o+ and h+ ions in the plasma sheet: Implications for the transport of ionospheric ions. *Journal of Geophysical Research*, *116*(A10). https://doi.org/10.1029/2011ja016532

Pitkänen, T., Kullen, A., Cai, L., Park, J.-S., Vanhamäki, H., Hamrin, M., et al. (2021). Asymmetry in the earth's magnetotail neutral sheet rotation due to imf b y sign? *Geoscience Letters*, *8*(1), 3. https://doi.org/10.1186/s40562-020-00171-7

Pollock, C., Moore, T., Jacques, A., Burch, J., Gliese, U., & Saito, Y. (2016). Fast plasma investigation for magnetospheric multiscale. *Space Science Reviews*, *199*, 331–406.

Raptis, S. (2024). Geomagnetic storms - Classified - 1993 - 2023. *Dataset] Zenodo*, *1*(0). https://doi.org/10.5281/zenodo.11407297

Regoli, L. H., Gkioulidou, M., Ohtani, S., Raptis, S., Mouikis, C. G., Kistler, L. M., et al. (2024). Temporal evolution of o+ population in the near-earth plasma sheet during geomagnetic storms as observed by the magnetospheric multiscale mission. *Journal of Geophysical Research: Space Physics*, *129*(5), e2023JA032203. https://doi.org/10.1029/2023JA032203

Runov, A., Angelopoulos, V., Sitnov, M., Sergeev, V., Nakamura, R., Nishimura, Y., et al. (2011). Dipolarization fronts in the magnetotail plasma sheet. *Planetary and Space Science*, *59*(7), 517–525. https://doi.org/10.1016/j.pss.2010.06.006

Russell, C., Anderson, B., Baumjohann, W., Bromund, K., Dearborn, D., Fischer, D., et al. (2016). Others (2016). The magnetospheric multiscale magnetometers. *Space Science Reviews*, *199*(1–4), 189–256. https://doi.org/10.1007/s11214-014-0057-3

Sciola, A., Merkin, V., Sorathia, K., Gkioulidou, M., Bao, S., Toffoletto, F., et al.(2023). The contribution of plasma sheet bubbles to stormtime ring current buildup and evolution of its energy composition. *Journal of Geophysical Research: Space Physics*, *128*(11), e2023JA031693. https://doi.org/10.1029/2023ja031693

Sitnov, M., Tsyganenko, N., Ukhorskiy, A., & Brandt, P. (2008). Dynamical data-based modeling of the storm-time geomagnetic field with enhanced spatial resolution. *Journal of Geophysical Research*, *113*(A7). https://doi.org/10.1029/2007ja013003

Sorathia, K., Michael, A., Merkin, V., Ohtani, S., Keesee, A., Sciola, A., et al. (2023). Multiscale magnetosphere-ionosphere coupling during stormtime: A case study of the dawnside current wedge. *Journal of Geophysical Research: Space Physics*, *128*(11), e2023JA031594. https://doi.org/10.1029/2023ja031594

Stephens, G., Sitnov, M., Kissinger, J., Tsyganenko, N., McPherron, R., Korth, H., & Anderson, B. (2013). Empirical reconstruction of storm time steady magnetospheric convection events. *Journal of Geophysical Research: Space Physics*, *118*(10), 6434–6456. https://doi.org/10.1002/jgra.50592

Tsyganenko, N., Singer, H., & Kasper, J. (2003). Storm-time distortion of the inner magnetosphere: How severe can it get? *Journal of Geophysical Research*, *108*(A5). https://doi.org/10.1029/2002ja009808

Vo, T., Ergun, R., Usanova, M., & Chasapis, A. (2023). Mesoscale structure and properties of the terrestrial magnetotail plasma sheet from the magnetospheric multiscale mission. *Journal of Geophysical Research: Space Physics*, *128*(9), e2023JA031358. https://doi.org/10.1029/2023ja031358

Wing, S., Johnson, J., Chaston, C., Echim, M., Escoubet, C., Lavraud, B., et al. (2014). Review of solar wind entry into and transport within the plasma sheet. *Space Science Reviews*, *184*(1–4), 33–86. https://doi.org/10.1007/s11214-014-0108-9

Wolf, R., Wan, Y., Xing, X., Zhang, J.-C., & Sazykin, S. (2009). Entropy and plasma sheet transport. *Journal of Geophysical Research*, *114*(A9). https://doi.org/10.1029/2009ja014044

Yang, J., Toffoletto, F. R., Wolf, R. A., & Sazykin, S. (2015). On the contribution of plasma sheet bubbles to the storm time ring current. *Journal of Geophysical Research: Space Physics*, *120*(9), 7416–7432. https://doi.org/10.1002/2015ja021398

Young, D., Burch, J., Gomez, R., De Los Santos, A., Miller, G., Wilson, P., et al. (2016). Hot plasma composition analyzer for the magnetospheric multiscale mission. *Space Science Reviews*, *199*(1–4), 407–470. https://doi.org/10.1007/s11214-014-0119-6

Zhou, X.-Z., Angelopoulos, V., Liu, J., Runov, A., & Pan, D.-X. (2014). Asymmetric braking and dawnward deflection of dipolarization fronts: Effects of ion reflection. *Geophysical Research Letters*, *41*(20), 6994–7001. https://doi.org/10.1002/2014gl061794